Electron transport in carbon nanotube shuttles and telescopes

I. M. Grace,* S. W. Bailey, and C. J. Lambert
Department of Physics, Lancaster University, Lancaster, United Kingdom
(Received 28 May 2004; published 27 October 2004)

Using a scattering technique, combined with density-functional theory, a computational study of the electron-transport properties of multiwall carbon nanotube (MWNT) telescopes and shuttles is presented. When the inner nanotube of a MWNT is displaced by an amount δx with respect to the outer tube, we predict that the interwall π-π coupling, $\gamma_{\pi\text{-}\pi}$, is significantly modified, leading to unexpected conductance oscillations for values of δx of the order of the interatomic spacing. An analytical model is presented, which provides a mapping between $\gamma_{\pi\text{-}\pi}$ and electron-transport measurements.

DOI: 10.1103/PhysRevB.70.153405 PACS number(s): 75.45.+j, 74.45.+c, 03.65.Sq

Multiwall carbon nanotubes (MWNTs) are coaxial cylinders with low translational and rotational energy barriers, which allow the inner tubes to easily slide with respect to the outer tubes.[1] This is demonstrated by recent experiments, which show that it is possible to slide the inner walls of a MWNT in a "telescoping"-like motion[2,3] and has led to the suggestion of low friction, MWNT-based nanoelectromechanical systems (NEMS), such as oscillators with frequencies in excess of 1 GHz.[4–6] For single wall nanotubes (SWNTs), electronic properties are primarily determined by chirality,[7] whereas in MWNTs the interwall interaction can cause the formation of pseudogaps[8] and in the case of telescoping nanotubes, resonances in the differential conductance of ballistic structures.[9–11] The aim of this article is to demonstrate that of all the naturally occurring MWNTs with random chiralities, there is a certain class of tubes, namely armchair-armchair double-wall NTs, which have the remarkable property of exhibiting large conductance oscillations as a function of an atomic-scale displacement between inner and outer tubes. Apart from the small fraction of naturally occurring examples, such structures could be engineered by starting from two single-wall armchair NTs and inserting one inside the other using a scanning probe tip. One consequence of our work is that in contrast with incommensurate MWNTs, such devices are predicted to be the ultimate nanoscale actuators, with an atomic-scale sensitivity.

We begin with an analysis of the electron transport properties of the telescoping MWNT shown in Fig. 1(a), as function of the displacement δx of the inner tube relative to the outer tube. Using a first principles approach, we predict that transport properties are strongly modified by displacements δx of order the interatomic spacing. By developing a minimal analytical model, which agrees well with the first-principles results, we also demonstrate that the strength of the interwall coupling can be probed experimentally by measuring the electrical conductance as a function of δx. Our analysis is also applied to the shuttle structure shown in Fig. 1(b), whose electronic properties are closely related to those of the corresponding telescope.

The problem of computing the δx dependence of the conductance is quite different from the problem considered in Ref. 10, which computes the energy dependence of the electron transmission coefficient for $\delta x=0$ only. To illustrate this, we note that since a NT is formed by repeatedly joining together identical slices of carbon atoms (which form the unit cells of the NT), the length L of the overlap region in a telescope can be written as $L=Nb+\delta x$, where b is the length of a slice of the inner or outer NT and δx is a displacement lying between $\pm b/2$ (i.e., $\delta x=L$ modulo b). For an infinite MWNT, the *ab initio*, mean-field Hamiltonian H is a periodic function of δx, with period b, and therefore to compute transport properties as a function of displacement, H must be recomputed self-consistently, for each value of δx.

The telescope shown in Fig. 1(a) comprises two coaxial SWNTS, with the inner NT connected to a SWNT extending to $+\infty$ and the outer NT connected to a larger diameter SWNT extending to $-\infty$. As a definite example, we focus on the armchair (6,6)@(11,11) MWNT, which has an interwall separation of 3.4 Å. This system is typical of most armchair MWNTs, as it does not possess axial symmetry. As a prelude to developing an analytical description, we first calculate transport properties using a recursive Green's function scattering technique, developed in Ref. 12, combined with a Hamiltonian generated using the first-principles density-functional theory code, SIESTA.[13] In what follows, we use the local density approximation parametrized by Perdue and Zunger[14] and nonlocal norm-conserving pseudopotentials.[15] The valence electrons are described by a single-ζ basis set. The cutoff radius for the s and p orbital is chosen to be 4.1 a.u.

Before computing transport properties, it is useful to examine the band structure of an infinite (6,6)@(11,11) MWNT. Since the Hamiltonian and overlap matrix elements depend on the positions of the carbon atoms of the inner NT relative to those on the outer NT, this band structure depends on the displacement δx of the inner NT relative to the outer NT. Figures 2(a) and 2(b) show the calculated band structure of an infinite, nondisplaced (6,6)@(11,11) MWNT, corresponing to $\delta x=0$.

Figure 2(a) shows that for positive k, in the vicinity of the Fermi energy, the band structure of the infinite MWNT possesses two π bands with positive slope and two π^* bands with negative slope. Several features of this band structure are relevant to understanding transport in telescopes and shuttles. First, as shown in Fig. 2(b), in the vicinity of the Fermi energy, small energy gaps of the order 2 meV, open at the band crossings. In what follows we demonstrate that oscillations in transport properties arise over a wide energy

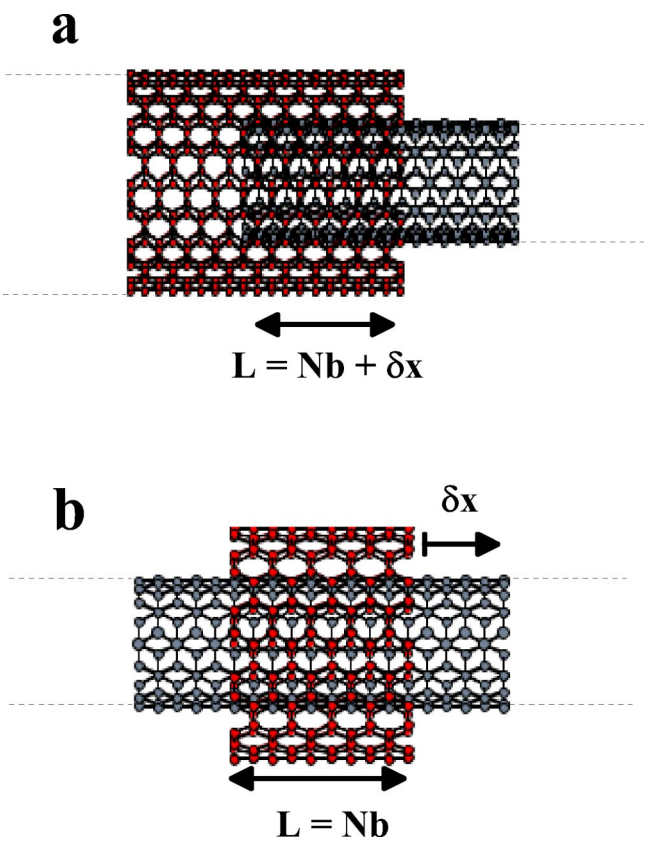

FIG. 1. (a) A telescoping MWNT in which a small-diameter NT is inserted a distance L into a larger diameter NT. The NTs are each connected to reservoirs on the left- and right-hand sides of the structures. In both cases, electrons are scattered at the points, separated by a distance L, where an NT terminates. (b) A "shuttle" system, in which a large-diameter SWNT (the shuttle) of length L is placed outside a small-diameter inner-wall NT, which in turn is connected to external reservoirs.

range and therefore these gaps are unimportant at most energies. Secondly, the π^* bands of the inner NT are shifted relative to those of the outer NT, mainly due to charge transfer between the NTs. This feature is demonstrated in Fig. 2(c), which shows the band structure arising when all matrix elements between orbitals on the outer NT and orbitals on the inner NT are artificially set to zero. In this case, the π bands are almost coincident, whereas the π^* bands on the different tubes remain shifted relative to each other. Finally, the π band of the inner NT is shifted relative to that of the outer NT, mainly due to the interwall interaction. This is

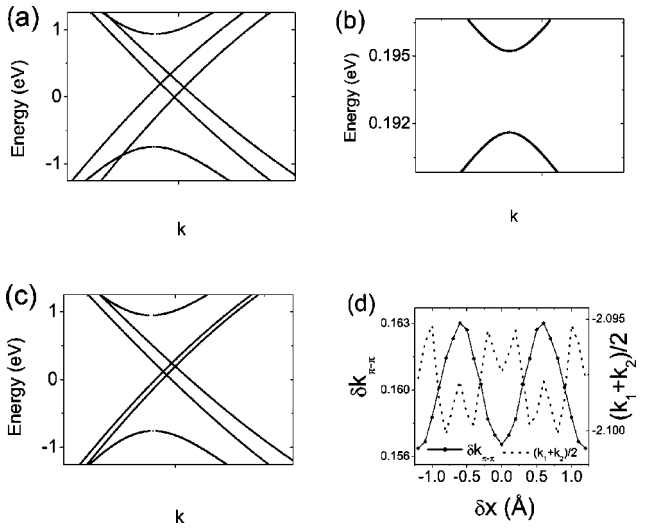

FIG. 2. (a) *Ab initio* (6,6)@(11,11) band structure close to the Fermi energy (0 eV). (b) Gap opening due to interwall interaction. (c) Band structure with no interwall interaction. (d) The difference $\delta k_{\pi\text{-}\pi}=k_2-k_1$ and average of the Fermi wave vectors k_1 and k_2 in the π bands as a function of δx.

demonstrated by the fact that the main effect of switching on the interwall matrix elements [i.e., in going from Figs. 2(a)–2(c)] is to shift the π bands, whilst leaving the others almost unaffected. The latter feature is crucial, since it produces large π-π scattering in telescopes and shuttles, while scattering involving other channels remains negligible. In view of the linearity of the bands near E_F, the wave-vector difference $\delta k_{\pi\text{-}\pi}=k_2-k_1$ between the two π bands is almost independent of energy. However, the Fermi wave vectors k_1 and k_2 of the π bands are extremely sensitive to the displacement δx of the inner tube relative to the outer tube. This is illustrated in Fig. 2(d), which shows the dependence of $\delta k_{\pi\text{-}\pi}$ and $(k_1+k_2)/2$ on δx. For such an infinite MWNT, these quantitites are periodic functions of δx, with period equal to the repeat distance $b=2.45$ Å of the MWNT.

Having examined band structure as a function of displacement δx, we now turn to transport properties of the telescoping (6,6)@(11,11) double-wall NT and demonstrate that the above δx dependence of the π wave vectors is accessible via conductance measurements on a telescope or shuttle. For scattering regions of length $L=Nb+\delta x$, Figs. 3(a) and 3(b) and [Figs. 4(a) and 4(b)] show *ab initio* results for the electrical conductance $G(E_F)=T(E_F)$ in units of $2e^2/h$ as a function of δx, for a telescope (shuttle) with two values of the

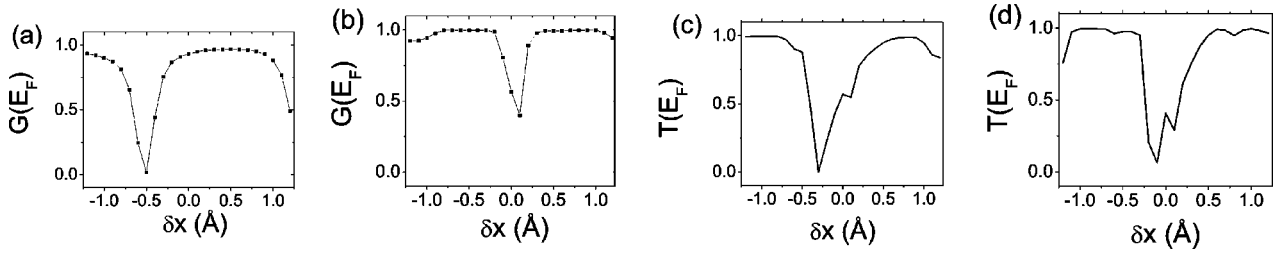

FIG. 3. *Ab initio* conductance $G(E_F)$ as a function of δx in a (6,6)@(11,11) telescope for scattering regions of length (a) $N=10$, and (b) $N=250$. Analytic description of $T(E)$ for the telescope model of length (c) $N=10$ and (d) $N=250$.

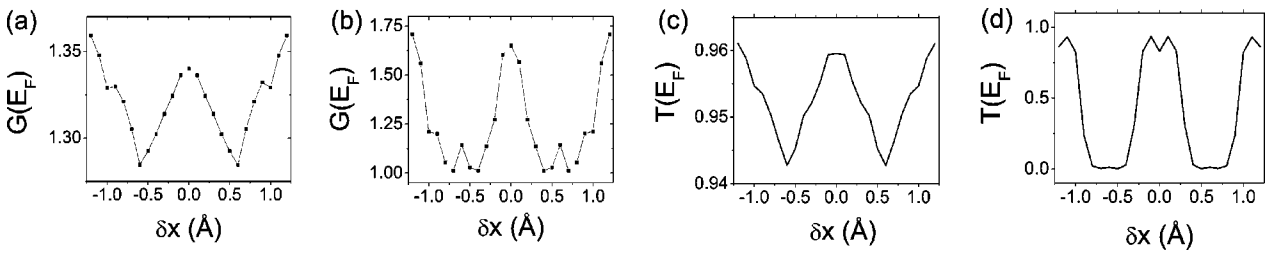

FIG. 4. (a) *Ab initio* conductance of the shuttle (6,6)@(11,11) nanotube as a function of δx for scattering lengths (a) $N=10$ and (b) $N=250$. Analytic desciption of transmission for the shuttle model of lengths (c) $N=10$ and (d) $N=250$.

number of over-lapping slices N. Perhaps the most striking feature of these results is the presence of large oscillations on the scale of $\delta x < b$. To demonstrate that these unexpected oscillations are a direct consequence of the δx dependence of the Hamiltonian, we now develop an analytical description of these oscillations based on retaining only the π-π interwall coupling. This approximation is partly justified by comparing Figs. 2(a) and 2(c), which show that switching on the interwall coupling yields a large shift in the π bands, while leaving the other bands almost unchanged. A restriction to π-π coupling is further suggested by comparing the energy dependence of the transmission coefficient of shuttles and telescopes. For $\delta x=0$, Fig. 5 shows the electron transmission coefficient $T(E)$ versus energy for fixed values of N. For energies in the approximate range ±1 eV, where only the π and π^* scattering channels are open, the transmission coefficient of the telescope (shuttle) oscillates between 0 and 1 (1 and 2). For higher energies, where four more scattering channels are open, these exhibit remarkably different behaviors, namely, $T(E)$ for the telescope continues to oscillate between 0 and 1, whereas $T(E)$ of the shuttle increases by 4 and oscillates between 5 and 6. This difference reflects the fact that for the telescope, only the π band of the outer tube scatters into the π band of the inner tube and no other channels are transmitted, whereas for the shuttle, only the π band of the inner tube is scattered by the presence of the shuttle, while all other channels are transmitted with a probability of almost unity.

In view of these results, we develop a minimal description of transport in telescopes (and shuttles), based on π-π scattering, which captures the essential physics of charge transfer and interwall coupling. The model is shown in Fig. 6, where a "circle" at position j represents the amplitude of a π state on slice j of one of the nanotubes. For a telescope, slices numbered $-\infty < j \leq N$ belong to the outer NT and slices $N+1 \leq j < \infty$ belong to the inner NT. For a shuttle, slices $N+1 \leq j \leq 2N$ belong to the inner NT and all others belong to the outer NT. In both cases, the Hamiltonian has diagonal matrix elements $H_{ii}=\varepsilon_0$ for $i \leq 0$ and $i \geq 2N+1, H_{ii}=\varepsilon_1$ for $1 \leq i \leq N$, and $H_{ii}=\varepsilon_2$ for $N+1 \leq i \leq 2N$, where the different values of ε_1 and ε_2 reflect the effect of charge transfer between the NTs. For sites $i,j \leq 0, i,j \geq N+1, 1 \leq i,j \leq N$, and $N+1 \leq i,j \leq 2N$, the nearest-neighbor π-π hopping matrix elements are set to $-\gamma$, while for $1 \leq i \leq N$, the interwall π-π coupling is $H_{i,i+N}=H_{i+N,i}=-\gamma_\pi$, where $\gamma_\pi < \gamma$. The coupling between the hybridized regions of length N slices and the left lead is $H_{0,1}=H_{1,0}=-\gamma_a$. For the shuttle (telescope) the coupling to the right lead is $H_{N,2N+1}=H_{2N+1,N}=-\gamma_b$, $(H_{2N,2N+1}=H_{2N+1,2N}=-\gamma_b)$. All other matrix elements are zero. In what follows, we find that good agreement with the *ab initio* results is obtained by allowing $\gamma_{\pi\text{-}\pi}$ to vary with δx, while all other parameters are independent of δx.

For both systems, the leads possess a dispersion relation $E=\varepsilon_0-2\gamma\cos k$ and feed electrons towards the hybridized region with a wave vector $k(E)=\cos^{-1}[(\varepsilon_0-E)/2\gamma]$ and group velocity $v(E)$ given by $\hbar v=dE/dk=2\gamma\sin k(E)$. The transmission coefficient from one lead to the other is given by $T(E)=[\hbar v(E)\gamma_a\gamma_b/\gamma^2]^2|G_{1\alpha}|^2$, where $\alpha=N$ for the shuttle, $\alpha=2N$ for the telescope, and G_{ij} is the retarded Green's function of the structure.

To compute G_{ij}, we start from Green's function g_{ij} of the disconnected structure arising when $\gamma_a=\gamma_b=0$. In this case, g_{00} is the Green's function on the right-most slice of the isolated semi-infinite left lead and $g_{2N+1,2N+1}=g_{00}$ is the

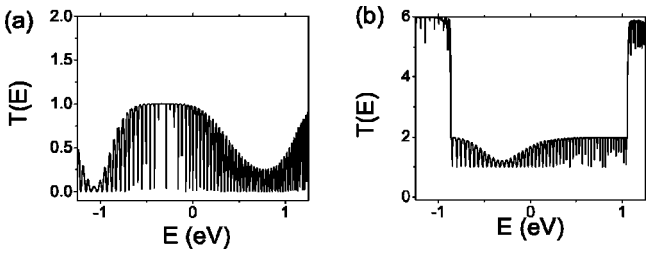

FIG. 5. Transmission coefficient vs energy for a telescope (a) and shuttle (b).

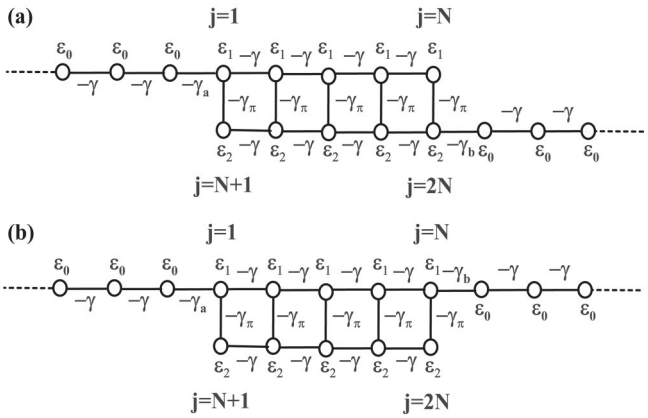

FIG. 6. Model representation of a (a) telescoping nanotube, and (b) shuttle nanotube.

Green's function on the left-most slice of the isolated semi-infinite right lead. The Green's function $G_{1\alpha}$ is then obtained by solving Dyson's equation,

$$G(E) = \left(\begin{pmatrix} g_{11} & g_{1\alpha} \\ g_{\alpha 1} & g_{\alpha\alpha} \end{pmatrix}^{-1} \begin{matrix} \gamma_a & 0 \\ 0 & \gamma_a \end{matrix} \right.$$
$$\left. \begin{matrix} \gamma_b & 0 \\ 0 & \gamma_b \end{matrix} \begin{matrix} g_{00}^{-1} & 0 \\ 0 & g_{00}^{-1} \end{matrix} \right)^{-1}. \quad (1)$$

In this expression, the surface Green's function of the isolated leads is $g_{00}=-\gamma^{-1}\exp 1k(E)$. To obtain the Green's function of the isolated hybridized region of length N, we introduce the wave vectors $k_1(E)$ and $k_2(E)$, defined to be solutions of

$$E = (\varepsilon_1 + \varepsilon_2)/2 - 2\gamma \cos k_j(E) - (-1)^j \sqrt{[(\varepsilon_1 - \varepsilon_2)/2]^2 + \gamma_\pi^2}. \quad (2)$$

In terms of these quantities, the Green's function of the isolated hybridized region of length N slices is given by $g_{11}=g_{NN}=A[c^2S(1,N)S(2,N+1)+s^2S(2,N)S(1,N+1)]$, $g_{2N+1,2N+1}=A[s^2S(1,N)S(2,N+1)+c^2S(2,N)S(1,N+1)]$, $g_{1N}=A[c^2S(1,1)S(2,N+1)+s^2\sin k_2 S(2,1)S(1,N+1)]$, and $g_{1,2N+1}=A[cs][S(1,1)S(2,N+1)-S(2,1)S(1,N+1)]$, where $s=\sin\theta, c=\cos\theta, S(i,j)=\sin k_i j, \cot\theta=-\gamma_\pi/[\sqrt{[(\varepsilon_1-\varepsilon_2)/2]^2+\gamma_\pi^2}]-(\varepsilon_1-\varepsilon_2)/2]$, and $A=-[2\gamma S(1,N+1)S(2,N+1)]^{-1}$. These expressions combine to yield

$$T(E) = \frac{4g_{1\alpha}^2(\gamma_a^2\gamma_b^2/\gamma^2)\sin^2 k(E)}{X + 4g_{1\alpha}^2(\gamma_a^2\gamma_b^2/\gamma^2)\sin^2 k(E)}, \quad (3)$$

where

$$X = [1 + g_{\alpha\alpha}^2\gamma_b^4/\gamma^2 + 2g_{\alpha\alpha}(\gamma_b^2/\gamma)\cos k - g_{1\alpha}^2\gamma_a^2\gamma_b^2/\gamma^2][1 + g_{11}^2\gamma_a^4/\gamma^2 + 2g_{11}(\gamma_a^2/\gamma)\cos k - g_{1\alpha}^2\gamma_a^2\gamma_b^2/\gamma^2] + [g_{11}\gamma_a^2/\gamma - g_{\alpha\alpha}\gamma_b^2/\gamma]^2. \quad (4)$$

For a given choice of the δx-independent parameters $\gamma_a/\gamma, \gamma_b/\gamma$, and $k(E_F)$, Eq. (3) provides a mapping between the δx-dependent parameters k_1, k_2, and θ of the infinite MWNT and the dimensionless conductance $T(E_F)$. Figure 2(d) shows that the δx dependence of the average $(k_1+k_2)/2$ is negligibly small (of order 0.1%), whereas $\delta k_{\pi\text{-}\pi}$ depends more strongly on δx. This can be modeled by allowing only $\gamma_{\pi\text{-}\pi}$ to vary with δx, while keeping ε_1/γ and ε_2/γ constant. In this way, the dependence of $T(E_F)$ on δx yields the δx dependence of $\gamma_{\pi\text{-}\pi}$ and vice versa.

To demonstrate this, we use the *ab initio* results of Fig. 2(d) for $\delta k_{\pi\text{-}\pi}$, to determine γ_π for each δx. For the clean limit, where $\gamma_a/\gamma=\gamma_b/\gamma=1$, choosing ε_1 and ε_2 to yield the correct zero-coupling π-band structure near E_F, shown in Fig. 2, and substituting these into Eq. (3), yields the analytic results shown in Figs. 3(c), 3(d), 4(c), and 4(d). These demonstrate that the above analysis based on π-π scattering yields good agreement with a first-principles description, and therefore, the nonmonotonic behavior in the conductance as a function of δx can be used to extract the electronic inter-wall coupling from conductance measurements.

The authors acknowledge support from the EPSRC and the EU research network MRTN-CT-2003-504574 RT-NNANO. We also thank Jaime Ferrer and Stefano Sanvito for useful discussions regarding SIESTA.

*Electronic address: i.grace@lancaster.ac.uk

[1] B. Bourlon, D. C. Glattli, C. Miko, L. Forró, and A. Bachtold, Nano Lett. **4**, 709 (2004).
[2] J. Cummings and A. Zettl, Science **289**, 602 (2000).
[3] M.-F. Yu, B. I. Yakobson, and R. S. Ruoff, J. Phys. Chem. B **104**, 8764 (2000).
[4] Q. Zheng and Q. Jiang, Phys. Rev. Lett. **88**, 045503 (2002).
[5] S. B. Legoas *et al.*, Phys. Rev. Lett. **90**, 055504 (2003).
[6] J. L Rivera, C. McCabe, and P. T. Cummings, Nano Lett. **3**, 1001 (2003).
[7] J. W. Mintmire, B. I. Dunlap, and C. T. White, Phys. Rev. Lett. **68**, 631 (1992).
[8] Y. K. Kwon and D. Tomanek, Phys. Rev. B **58**, R16001 (1998).
[9] S. Sanvito, Y. K. Kwon, D. Tomanek, and C. J. Lambert, Phys. Rev. Lett. **84**, 1974 (2000).
[10] D.-H. Kim and K. J. Chang, Phys. Rev. B **66**, 155402 (2002).
[11] D.-H. Kim, H.-S. Sim, and K. J. Chang, Phys. Rev. B **64**, 115409 (2001).
[12] S. Sanvito, C. J. Lambert, J. H. Jefferson, and A. Bratkovsky, Phys. Rev. B **59**, 11936 (1999).
[13] J. M. Soler, E. Artacho, J. D. Gale, A. Garca, J. Junquera, P. Ordejn, and D. Sanchez-Portal, J. Phys.: Condens. Matter **14**, 2745 (2002).
[14] J. P. Perdew and A. Zunger, Phys. Rev. B **23**, 5048 (1981).
[15] N. Troullier and J. L. Martins, Phys. Rev. B **43**, 1993 (1991).